# Numerical Methods of Thermo-Fluid Dynamics II

Summer Semester 2021

## Deliverable Task I:

## Large Eddy Simulation of Flow Over a Circular Cylinder at Re = 3900

Submitted by:


Serouj Djabraian
Matrikelnummer 22849126
serouj.d.djabraian@fau.de

Franciskus Xaverius Erick
Matrikelnummer 22811754
franciskus.erick@fau.de

Prashanth Prakash Kamath
Matrikelnummer 22835087
prashanth.kamath@fau.de

John Sebert Mampilli
Matrikelnummer 22833931
john.mampilli@fau.de

Sudesh Rathnayake Mudiyanselage
Matrikelnummer 22849910
sudesh.rathnayake@fau.de

# Introduction

The objective of Deliverable Task I was to simulate the flow over a circular cylinder using the free and open-source CFD software OpenFOAM, with the pimpleFoam solver and Large Eddy Simulation (LES). The computational domain consisted of a circular cylinder of diameter $D = 5\,\text{cm}$, placed inside a concentric circular domain of diameter $L = 30D$.

The boundary conditions specified were:

- No-slip condition at walls
- Velocity: uniform streamwise velocity at inlet (Dirichlet boundary) and zero-gradient at outlet (Neumann boundary)
- Pressure: zero-gradient at inlet and outlet (Neumann boundaries)
- Symmetry boundary conditions were used at the front and back planes of the domain.

The Reynolds number and kinematic viscosity were specified in the problem definition as $Re = 3900$ and $\nu = 1.0023 \times 10^{-6}\,\text{m}^2/\text{s}$ respectively. Correspondingly, the inlet velocity was calculated as $\vec{V} = (0.0781794, 0, 0)\,\text{m/s}$.

# 1. Summary of LES and Smagorinsky Model

For LES simulations, OpenFOAM solves the following equation.

$$\frac{\partial \bar{u}_i}{\partial t} + \frac{\partial}{\partial x_j}(\bar{u}_i \bar{u}_j) = -\frac{1}{\rho}\frac{\partial \bar{p}}{\partial x_i} + \nu \frac{\partial}{\partial x_j}(\frac{\partial \bar{u}_i}{\partial x_j} + \frac{\partial \bar{u}_j}{\partial x_j}) - \frac{\partial \tau_{ij}^{SGS}}{\partial x_j} \tag{1.1}$$

Whereby $\bar{u}_i$,$\bar{u}_j$ and $\bar{p}$ are grid-scale filtered velocity vectors and filtered pressure. The filtering process in OpenFOAM is done implicitly using top-hat filter. $\tau_{ij}^{SGS}$ is the sub-

grid scale stress-tensor which models the small scales behavior. For general Smagorinsky models, this term is expressed to be proportional to the grid scale deformation tensor $S_{ij}$.

$$\tau_{ij}^{SGS} = -2\nu_t \bar{S}_{ij} \quad \text{, with} \quad S_{ij} = \frac{1}{2}(\frac{\partial \bar{u}_i}{\partial x_j} + \frac{\partial \bar{u}_j}{\partial x_j}) \tag{1.2}$$

The term $\nu_t$ is an introduced eddy viscosity term which is solely used to model the small-scales turbulent behavior of the fluid. By substituting 1.2 to 1.1, the Navier-Stokes equation to be solved can then be expressed as follows.

$$\frac{\partial \bar{u}_i}{\partial t} + \frac{\partial}{\partial x_j}(\bar{u}_i \bar{u}_j) = -\frac{1}{\rho}\frac{\partial \bar{p}}{\partial x_i} + (\nu + \nu_t)\frac{\partial}{\partial x_j}(\frac{\partial \bar{u}_i}{\partial x_j} + \frac{\partial \bar{u}_j}{\partial x_j}) \tag{1.3}$$

For the Smagorinsky model of OpenFOAM, the term $\nu_t$ is evaluated as follows [1].

$$\nu_t = C_k \Delta k^{0.5} \tag{1.4}$$

The term $\Delta$ is the filter length scale. The term $k$ refers to the turbulence kinetic energy, which is to be solved from the following quadratic equation.

$$ak^2 + bk + c = 0 \tag{1.5}$$

And the coefficient terms $a$, $b$, and $c$ are in turn evaluated as follows.

$$a = \frac{C_e}{\Delta}$$

$$b = \frac{2}{3}\mathrm{tr}(\mathbf{D})$$

$$c = 2C_k \Delta(\mathrm{dev}(\mathbf{D}) : \mathbf{D})$$

The matrix $\mathbf{D}$ is evaluated from the gradients of the velocity vectors as follows.

$$\mathbf{D} = \frac{1}{2}(\nabla \mathbf{u} + \nabla(\mathbf{u})^T)$$

The calculation of the coefficient terms include the trace operator "tr" that calculates the trace ( product of diagonals ) of the tensor $\mathbf{D}$ and the deviatoric operator "dev" that extracts the deviatoric component of the tensor $\mathbf{D}$. The default value of the coefficent $C_e$ is 1.048, while the default value of the coefficient $C_k$ is 0.094.

# 2. Grid Convergence Study

In order to study grid convergence, the transient simulation was performed on all the provided meshes, up to an end time of 1000 s. The recirculation lengths were then calculated on all the meshes. The resolutions of the provided meshes and the obtained recirculation lengths were:

| Mesh # | Resolution | Recirculation Length $L_r$ (m) |
|---|---|---|
| Mesh 0 | $75 \times 165 \times 10$ | 0.054000 |
| Mesh 1 | $98 \times 165 \times 10$ | 0.054750 |
| Mesh 2 | $127 \times 165 \times 10$ | 0.051825 |
| Mesh 3 | $165 \times 165 \times 10$ | 0.052500 |

The mesh refinement ratio was given as $r = 1.3$. Using the values of $L_r$ and $r$, the order of convergence was calculated using equation (2.1) [2].

$$p = \frac{1}{ln(r)} \times \left( ln \left| \frac{\Phi_3 - \Phi_2}{\Phi_2 - \Phi_1} \right| \right) \tag{2.1}$$

In equation (2.1), $\Phi$ is the variable of interest ($L_r$ in this case), and the subscripts 1, 2 and 3 refer respectively to meshes in decreasing order of refinement, i.e. 1 refers to the finest mesh, and 3 refers to the coarsest.

Next, the relative error and grid convergence index (GCI) were calculated using equations (2.2) to (2.5) [2],

$$\epsilon^{21} = \left| \frac{\Phi_1 - \Phi_2}{\Phi_1} \right| \tag{2.2}$$

$$\epsilon^{32} = \left| \frac{\Phi_2 - \Phi_3}{\Phi_2} \right| \tag{2.3}$$

$$GCI^{21} = \frac{F_s \cdot \epsilon^{21}}{r^p - 1} \tag{2.4}$$

$$GCI^{32} = \frac{F_s \cdot \epsilon^{32}}{r^p - 1} \tag{2.5}$$

where $F_s = 1.25$.

The decision of which mesh to use was made based on whether the meshes yield solutions that are in the asymptotic range of convergence. This was checked using (2.6).

$$\frac{GCI^{32}}{r^p \cdot GCI^{21}} \approx 1 \tag{2.6}$$

Equation (2.6) was found to hold for Meshes 1, 2 and 3, and hence Mesh 2 was chosen to carry out further calculations and post-processing.

# 3. Running pimpleFoam Efficiently – Pressure and Velocity Relaxation Factors

Four pairs of relaxation factors for the velocity equations and pressure field were tested, to study the effect of relaxation factors on the number of outer iterations required until convergence. The relaxation factors used and the number of outer iterations required are given in table 2.

| Relaxation Factors (U, p) | Outer Iterations Required |
|---|---|
| (0.5, 0.5) | 18 |
| (0.7, 0.7) | 11 |
| (0.8, 0.8) | 8 |
| (0.9, 0.9) | 6 |

The stability of the computations using the pair (0.9, 0.9) was studied by plotting the residuals (figures 3.1 and 3.2). As this pair required the fewest outer iterations to converge per timestep, and the simulation remained stable, it was chosen to be used for further computations.

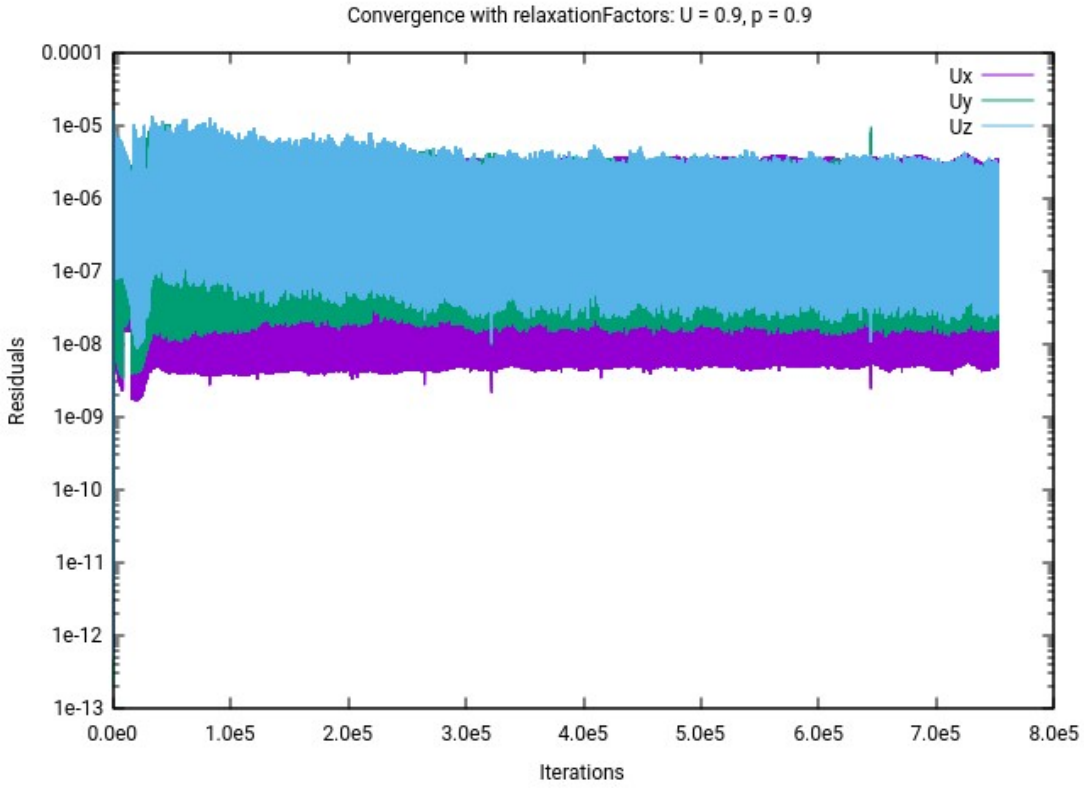


Figure 3.1: Residual plot of momentum equations

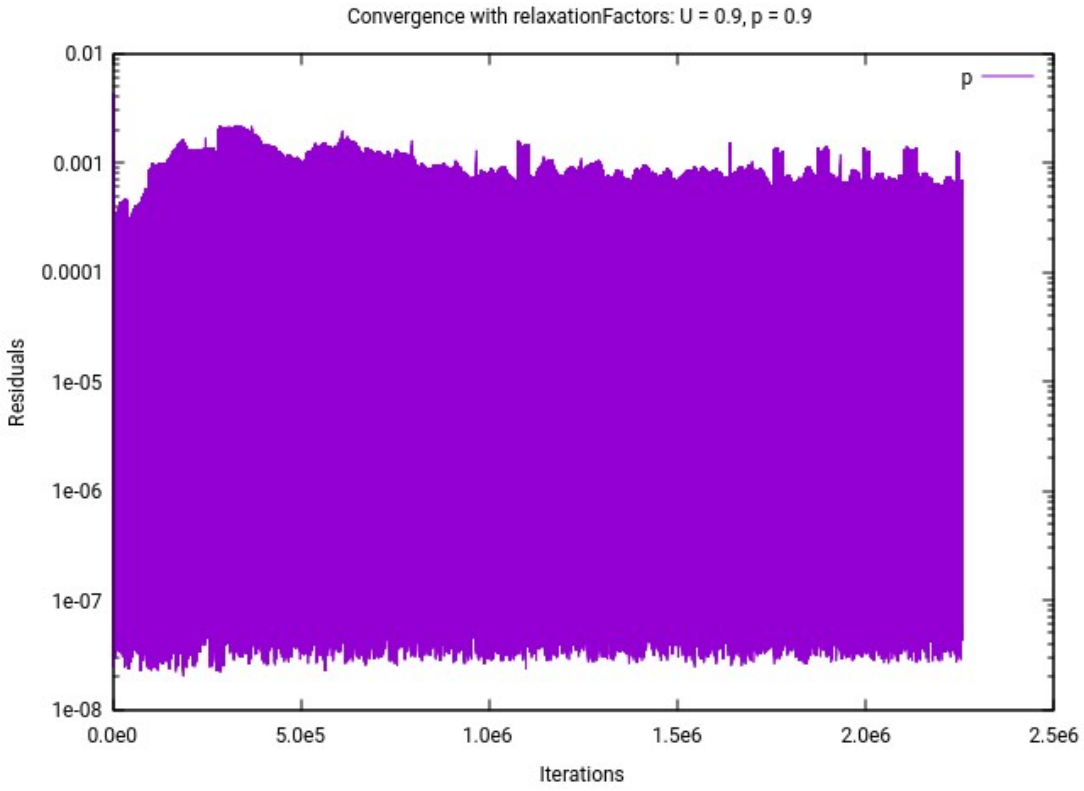


Figure 3.2: Residual plot of pressure equation

# 4. Theory Behind Vortex Shedding

Vortex shedding is the phenomena whereby vortices are formed when fluids flow past an object, especially bluff objects. When fluid flows past an object, the boundary layer near the object boundary continues downstream of the body. For streamlined objects, these boundary layer does not separate prematurely and the flow remains relatively intact downstream. However, for bluff objects, the flow near the boundary layer separates prematurely, forming vortices and a larger region of wake with higher turbulence. This formation of large region of drag also results to larger pressure drag for bluff bodies, as the pressure in the wake area downstream of the object is lower than the pressure upstream of the object. The kinetic energy of the flow is also decreased substantially due to the formation of turbulence and the following dissipation the occurs.

For a moderate value of Reynold's number, the shedding of vortices occurs alternatively and periodically on both upper and lower side of the object. This is known as Karman Vortex Street [3]. As the boundary layer grows larger, they separate from the main boundary layer itself and split as vortices in the wake region. The alternating shedding of vortices can be described as the interaction between the growth of the boundary layers from both sides of the objects. As one side of the boundary layer gets larger in the wake area, this increased boundary layer itself draws the flow of the fluid in the wake area from the other side of the object towards its direction, thus forcing the flow from the other side to recirculate slightly. Once the boundary layer from that one side gets to a certain size and split, the recirculated side would then have its boundary layer increase until the vortex is also shed from that side.

The alternating flow behaviours from both sides of the objects results to alternating pressure gradients from both sides of the object, which also create alternating lateral force from both sides of the object. The periodicity of vortex shedding is associated with a spectrum of shedding frequency values. The most dominant shedding frequency however is taken to be the main shedding frequency. Vortex shedding is generally described by the dimensionless quantity Strouhal number.

$$\mathrm{Sr} = \frac{f_s d}{u}$$

$f_s$ is the shedding frequency, $d$ is the characteristic length of the geometry, and $u$ is the flow velocity. For cylinders, the characteristic lenght is taken to be the diameter of the cylinder. For a smooth cylinder, vortex shedding can be classified into 4 regions depending on the Reynold's number of the flow[4]:

1. Below subcritical region ( $Re < 300$ ): Vortices start to develop more with increasing boundary layer size and the wake becomes more turbulent with increasing Reynold's number.

2. Subcritical region ( $300 < Re < 1.5x10^5$ ): The typical region where normal periodic vortex shedding occurs.

3. Transition region ( $1.5x10^5 < Re < 3.5x10^6$ ): Observed vortex shedding effect starts to diminish due to the increased range of shedding frequencies.

4. Supercritical region ( $Re < 3.5x10^6$ ): The boundary layer around the cylinder is now turbulent and vortex shedding effect reappears.

The effect of Reynold's number to Strouhal's number is additionally displayed in figure 4.1.

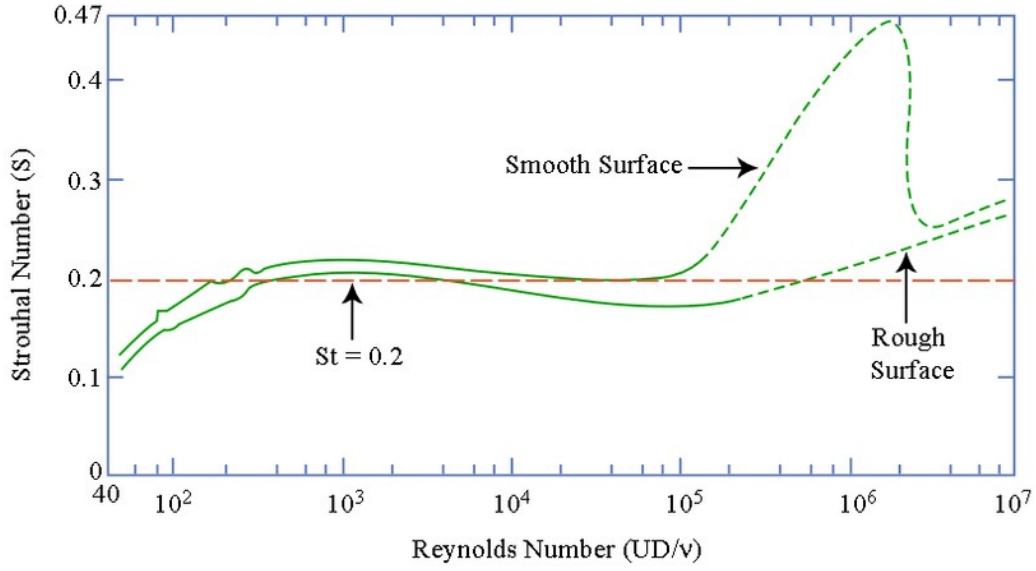


Figure 4.1: Strouhal number as a function of Reynold's number[5].

It can be easily seen that for any Reynold's number in the Reynold's number range given above, there are a range of Strouhal values corresponding to the range of shedding frequencies. When the most significant shedding frequency is equal or close to the resonance frequency of the object, the object may resonate. Thus, vortex shedding needs to

be taken into account when designing a structure or object as resonations may lead to structural failure.

# 5. Results and Interpretation

Data Analysis was done using Paraview. Figure 5.1 shows the magnitude of the velocity at the final time step for a total runtime of 1000 seconds. The velocity shown in this figure is the average velocity over all timesteps, which is a better parameter to consider, rather than considering instantaneous velocity components for our LES simulation.

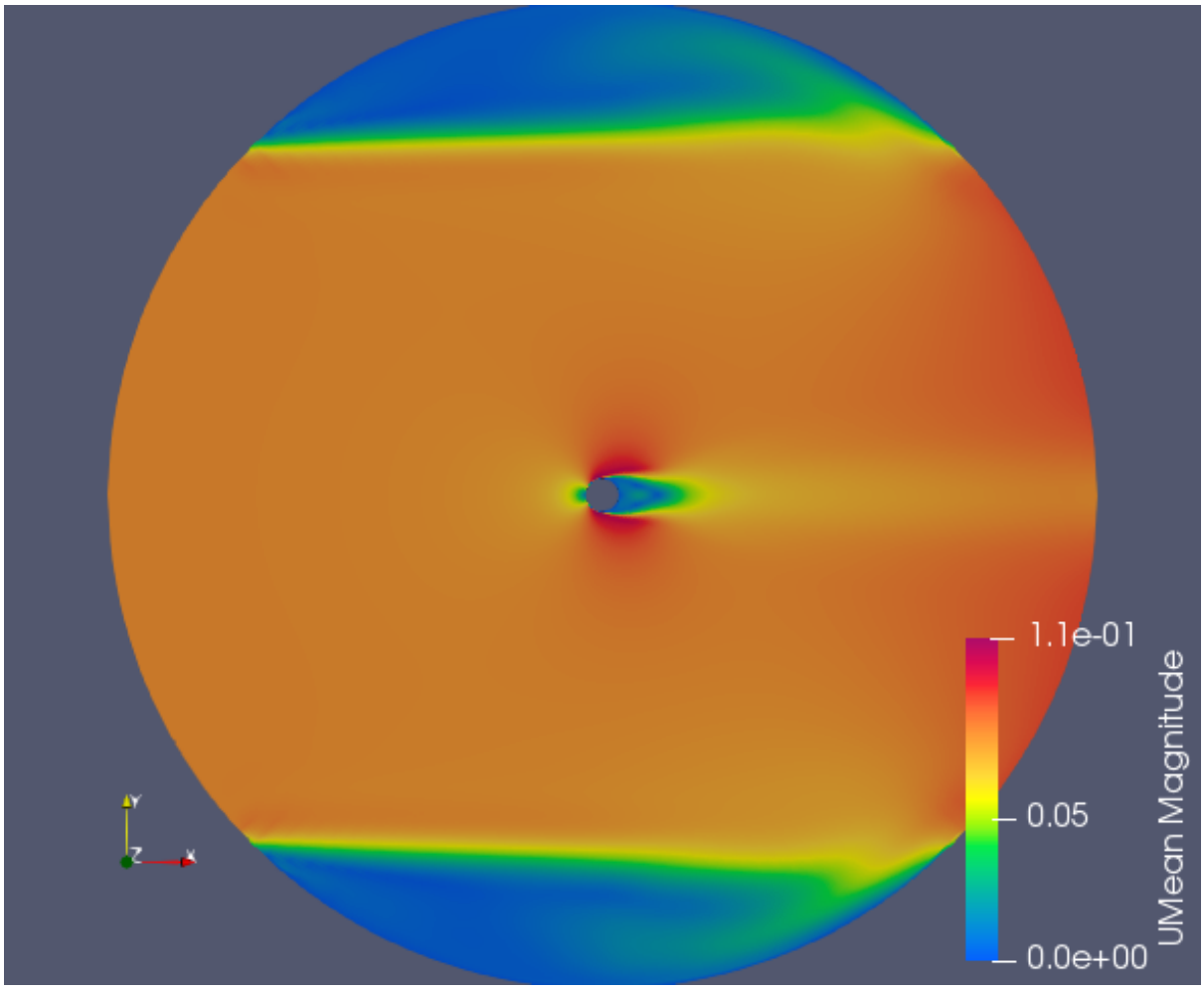


Figure 5.1: Representation of the mean velocity for the entire domain

In figure 5.2 a closer look into the velocity magnitude over the cylinder is observed with additional velocity contours which help differentiate areas with higher or lower velocities.

As seen the velocity is highest at the upper and lower surfaces of the cylinder, and there is a stagnation point on the cylinder where velocity is almost zero. Behind the cylinder is the formation of the wake region where the re-circulation occurs. The flow velocity in this region is low because of re-circulation and backflow.

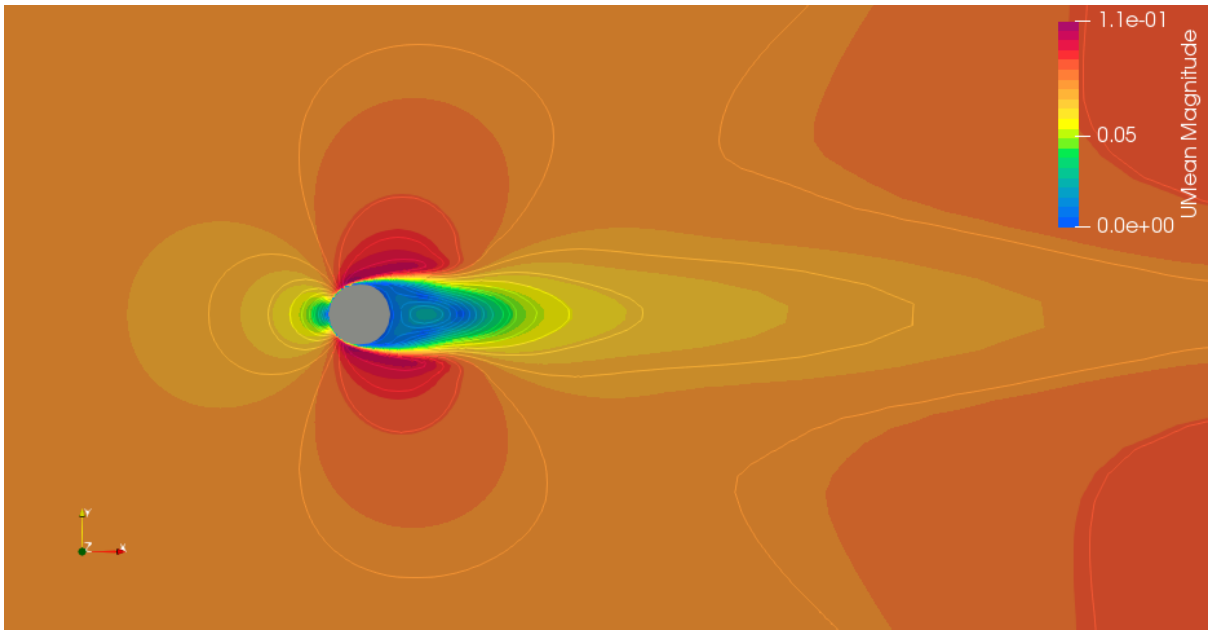


Figure 5.2: Representation of the velocity contours around the cylinder for mean velocity

Figures 5.3 and 5.4 show the variation of the $u$ and $v$ velocities which are represented by 'Ux' and 'Uy' in the figures. These figures were plotted by using the 'Plot Over Line' filter in Paraview, where the line was located in the wake region of the cylinder at $y = 0$. It can be seen that the $u$ velocity is 0 at the wall of the cylinder in the wake region, which marks our 2nd stagnation point behind the cylinder. As we move along the line, the flow is in the opposite direction which is due to re-circulation. Then at some point the velocity magnitude starts increasing until reaching a value of 0 again which is the end of our re-circulation zone. It then continues increasing until stabilizing. As for the $v$ velocity, it can be seen that its magnitude is fluctuating on the entire line, it is more or less unpredictable and gives us a glimpse of how the vortex shedding occurs.

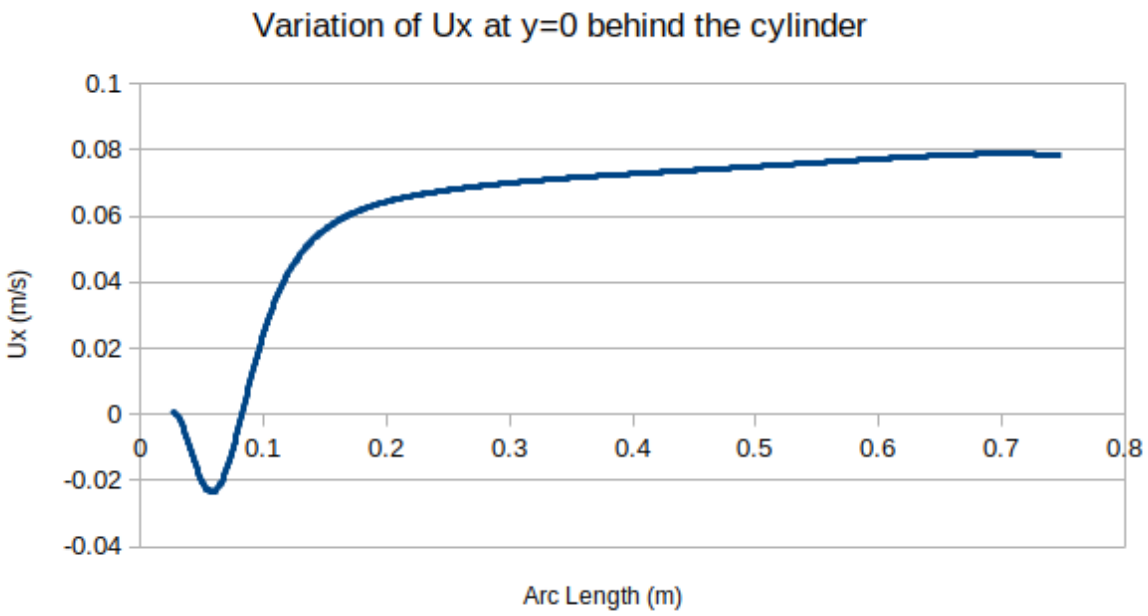


Figure 5.3: Variation of Ux at $y = 0$ behind the cylinder

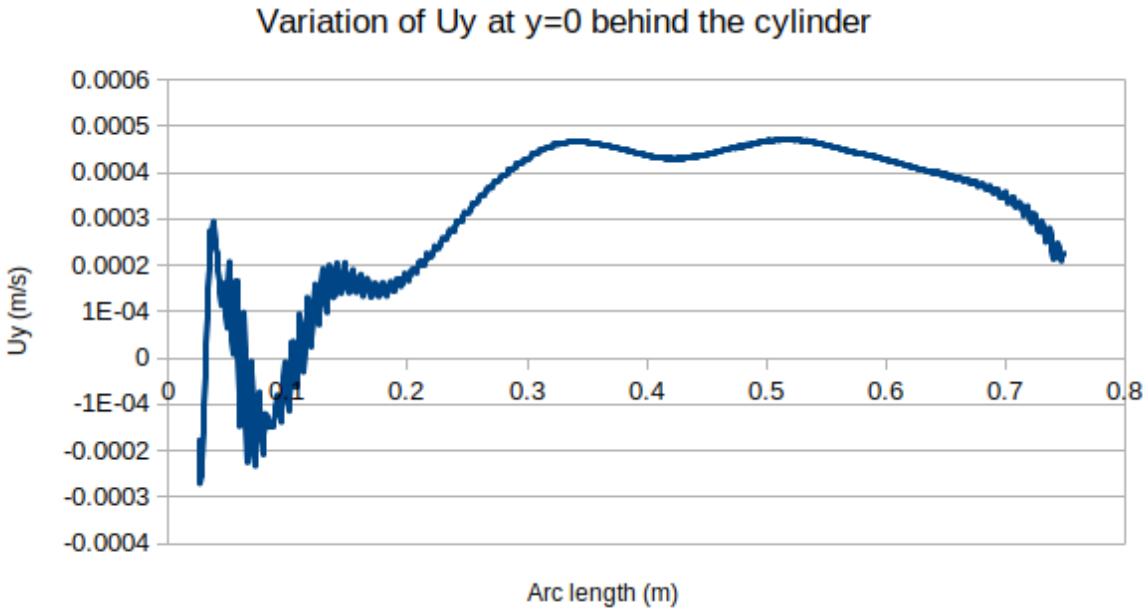


Figure 5.4: Variation of Uy at $y = 0$ behind the cylinder

Figure 5.5 shows the instantaneous streamwise velocity streamlines. It can be seen that the streamlines are following an unpredictable and turbulent pattern, which is due to the eddies that are being created in the wake region of the cylinder. Moreover, we can see the re-circulation region forming right behind the cylinder from the streamlines. Similarly in figure 5.6, we can observe the mean streamwise velocity streamlines. It can be seen the the streamlines follow an almost laminar pattern in the wake region in addition to a re-circulation region behind the cylinder. This phenomenon is due to the velocity averaging over time.

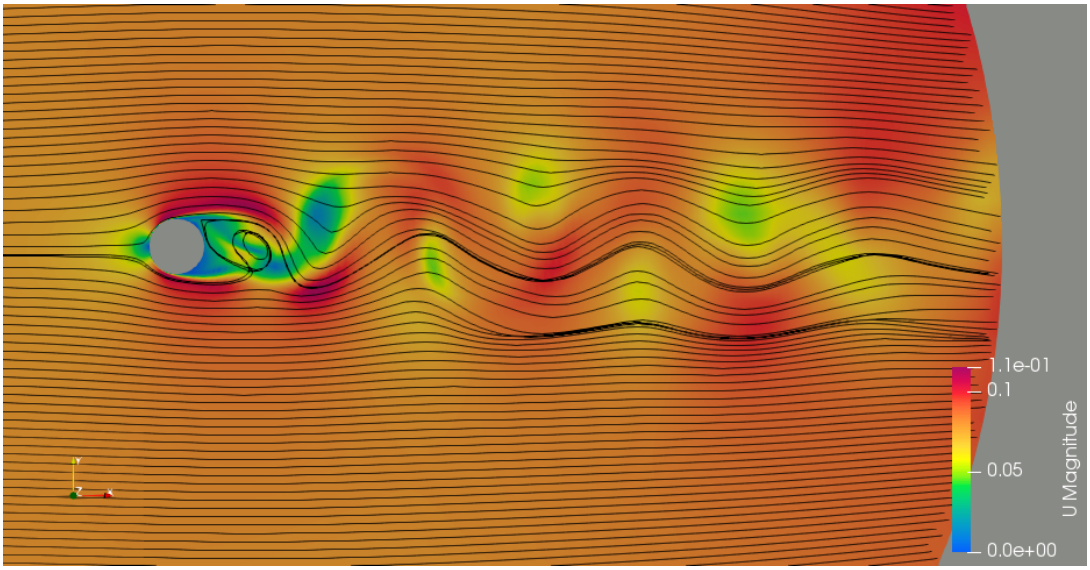


Figure 5.5: Instantaneous streamwise velocity streamlines

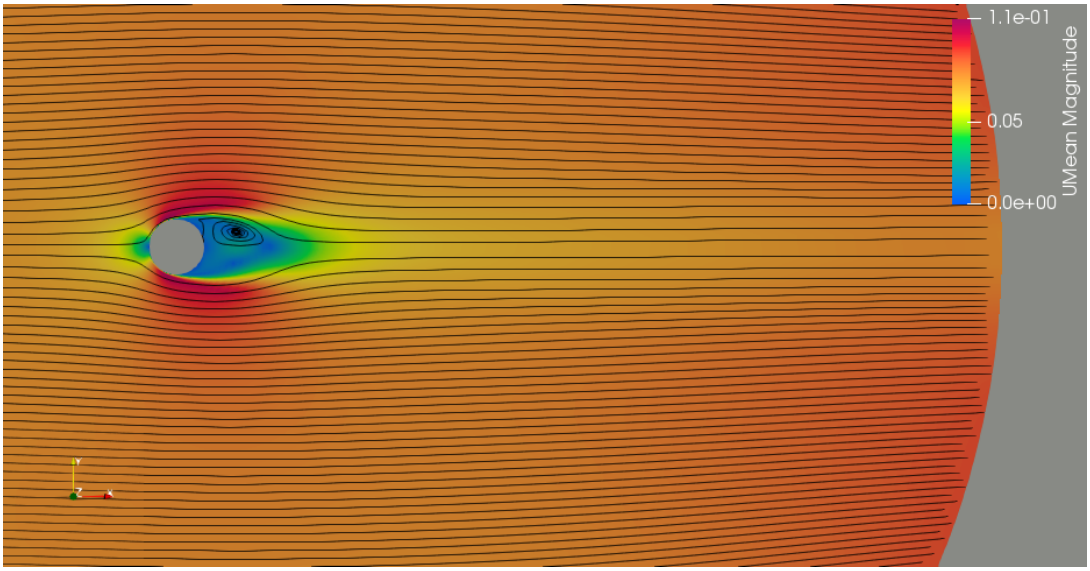


Figure 5.6: Mean streamwise velocity streamlines

## Calculation of Wall Shear Stress

In order to calculate the shear stress at the wall of the cylinder, we need to implement the following relation:

$$\tau_w = \mu \cdot \frac{du}{dy}$$

In order to calculate the gradient at the wall, in Paraview a 'Plot on Intersection Curves' filter was used in cylindrical shape, where the the values of the velocities were extracted for the very first grid point close to the wall. Multiplying the gradient of the velocity on the wall with the dynamic viscosity of water which is roughly $1 \times 10^{-3}\,\mathrm{kg/(m\,s)}$ at 20 °C, we get figure 5.7 for the wall shear stress.

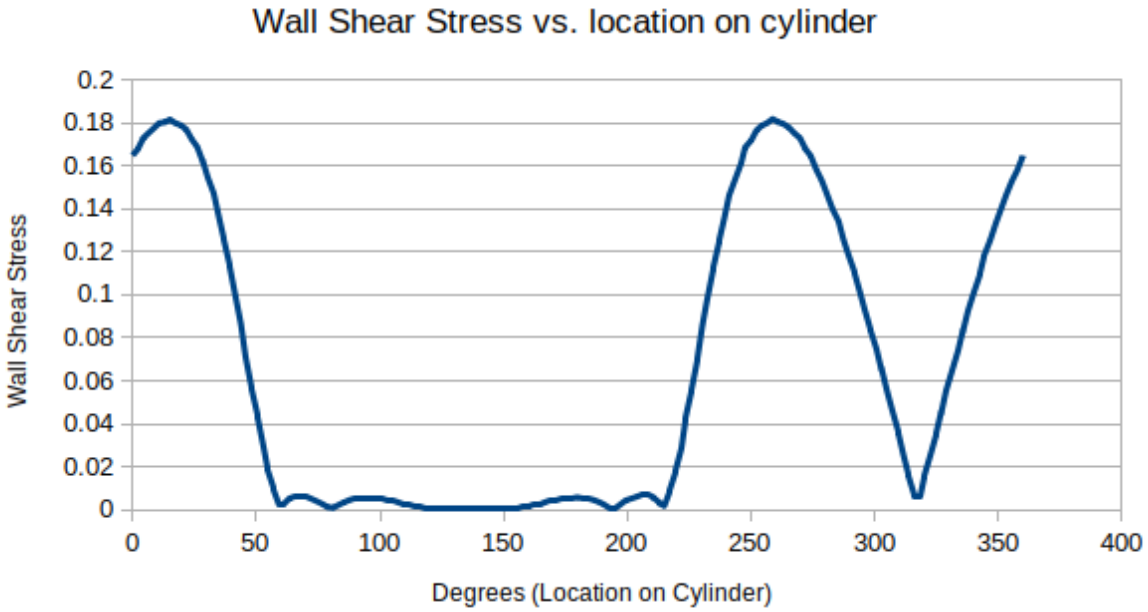


Figure 5.7: Representation of the wall shear stress

From figure 5.7, we can see a large region where wall shear stress is equal to zero, and this is the wake region where the flow has separated. At approximately 320° we have the stagnation point where the wall shear stress is also zero because of zero velocity gradient. Thus we can see that the flow separates at some point on the cylinder, where the wall shear stress hits zero.

## Friction Coefficient

To calculate the friction coefficient we implement the following formula:

$$C_f = \frac{\tau_w}{0.5 \cdot \rho U_\infty^2}$$

With the values of the wall shear stress calculated previously, we get the plot shown in figure 5.8. This plot behave similarly to the wall shear stress, where we can also recognize the flow separation point, since the parameters used to calculate the friction coefficient are nothing but scaling factors.

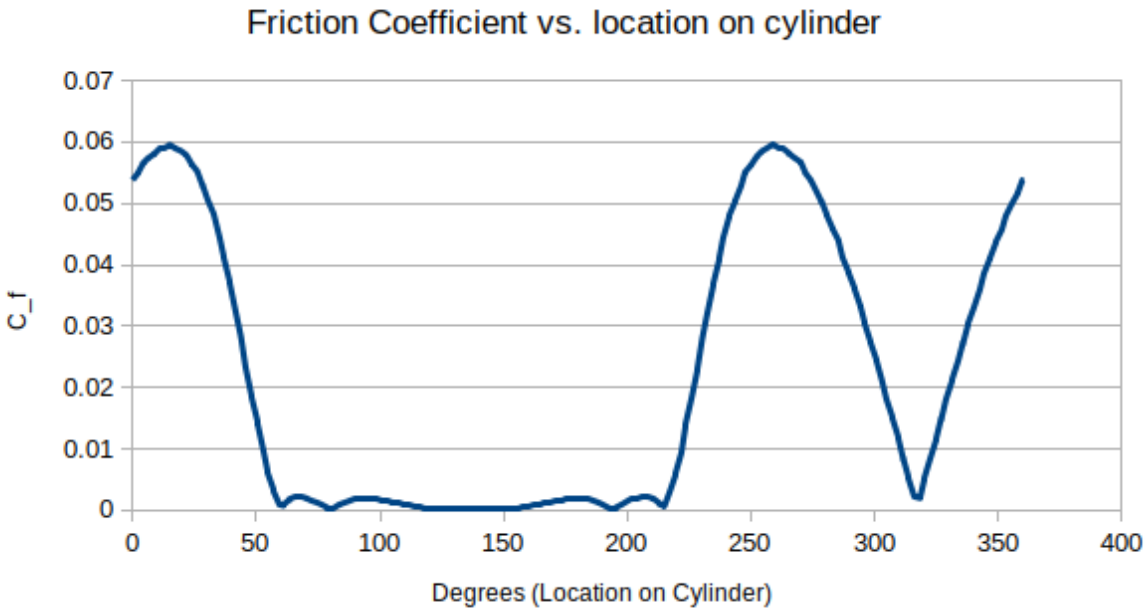


Figure 5.8: Friction coefficient plot

## Pressure Coefficient

To calculate the pressure coefficient we implement the following formula:

$$C_p = \frac{P - P_\infty}{0.5 \cdot \rho U_\infty^2}$$

where the numerator is the pressure scalars calculated by OpenFOAM divided by the local density of the cells. Thus we will not include the density value in this formula, then we get the plot in figure 5.9, where it can be seen that we have positive values in front of the cylinder and negative values behind the cylinder.

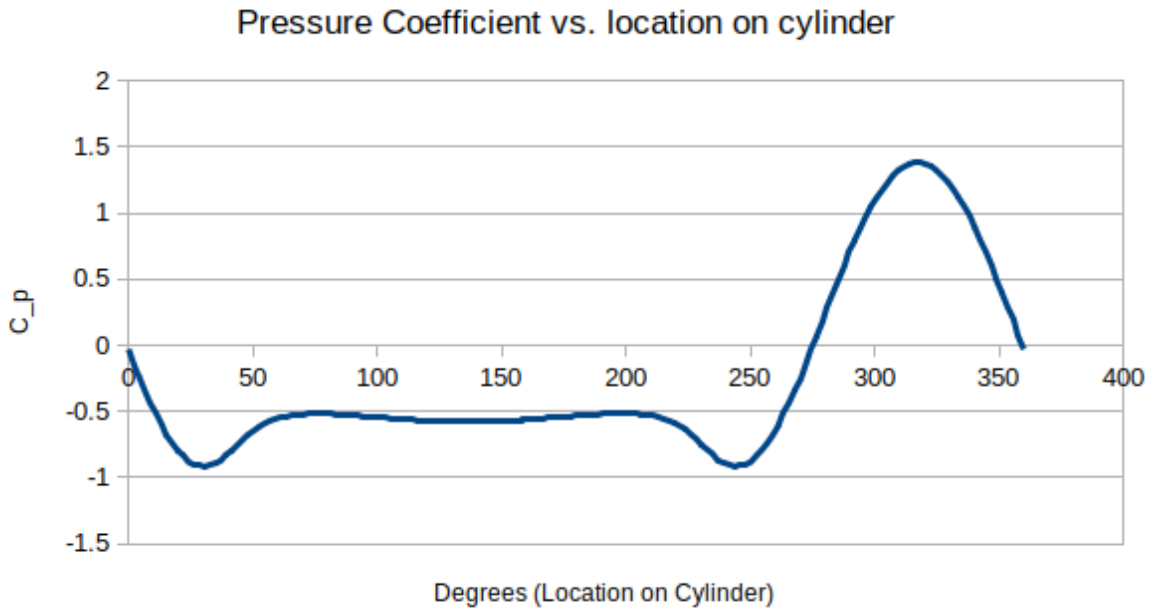


Figure 5.9: Pressure coefficient plot

## Lift and Drag Coefficients

To calculate the lift and drag coefficients, we implement the following formulas:

$$C_l = \frac{F_l}{0.5 \cdot \rho A U_\infty^2} \qquad C_d = \frac{F_d}{0.5 \cdot \rho A U_\infty^2}$$

In order to calculate the lift and drag forces, we need to find the pressure forces acting on the surface of the cylinder, multiply these forces with the respective vectors (x-direction for drag and y-direction for lift), and then we need to integrate all of these values in order to get total force acting on the cylinder. The area in this equation is nothing but the cross-sectional area of the cylinder. Moreover, we need to calculate the forces for every time step. Performing the mentioned methods, we get the plots in figures 5.10 and 5.11 for the lift and drag coefficients respectively.

It can be seen in figures 5.10 and 5.11 that the drag coefficient starts at a certain value at the first time step, and then it starts stabilizing at a value of 1 after 50 seconds of runtime. For the lift coefficient, it can be seen that it is equal to zero until the flow develops, but then it starts fluctuating from negative lift to positive lift from one timestep to another, which is a phenomena of vortex shedding. Note that the maximum total time was reduced to certain values of order to better visualize the variation of the lift and drag coefficients.

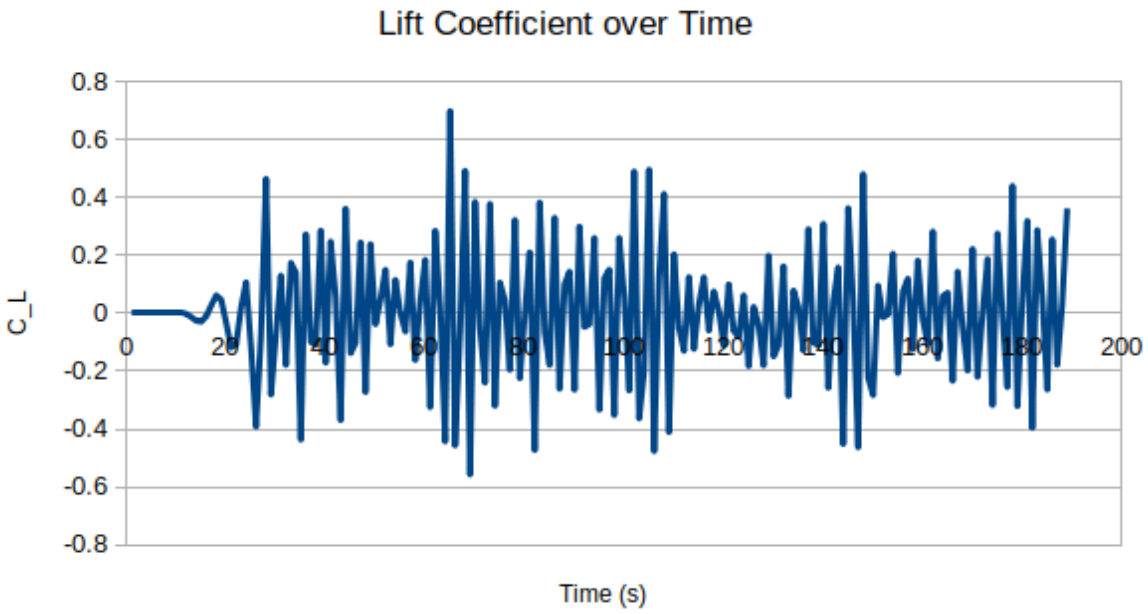


Figure 5.10: Lift coefficient

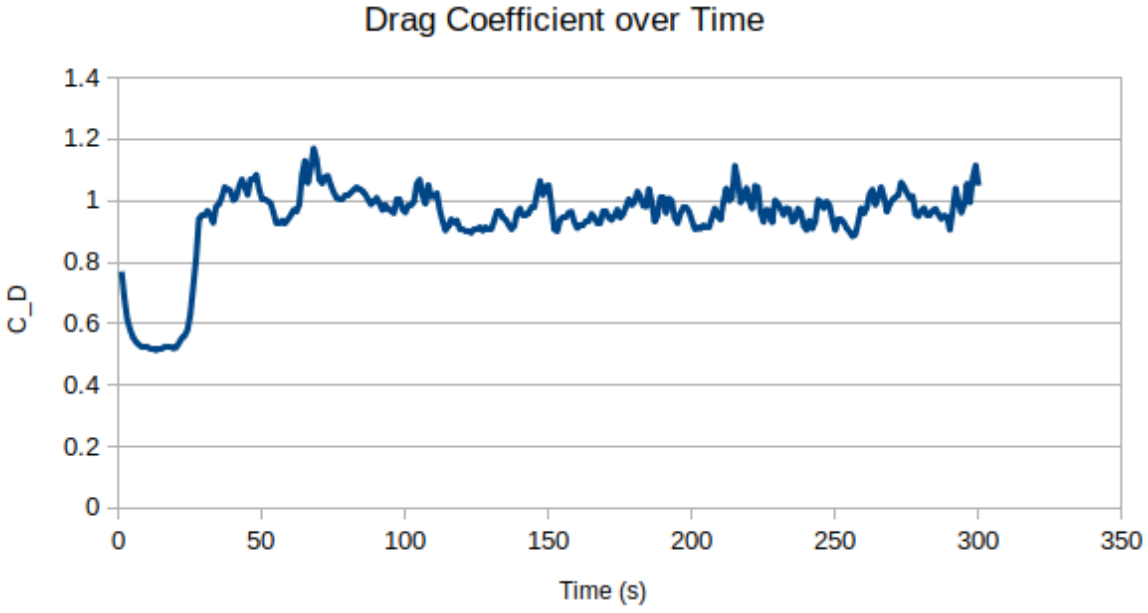


Figure 5.11: Drag coefficient

## Strouhal Number

The Strouhal number is commonly used as a parameter to measure the dominant shedding frequency at which vortex shedding occurs. It is represented by the following formula:

$$Sr = \frac{f_s \cdot L}{U_\infty}$$

where $f_s$ is the frequency of the vortex shedding, $U_\infty$ is the freestream velocity and $L$ is the characteristic length of the cylinder (Diameter).

In order to calculate the Strouhal number, we need to first calculate the vortex shedding frequency. This calculation can be done by performing a Fast Fourier Transform (FFT) of the lift coefficient plot that we just computed. The FFT of the lift coefficient will output the maximum amplitude of the frequency at which vortex shedding occurs. Implementing the FFT produces the plot in figure 5.13.

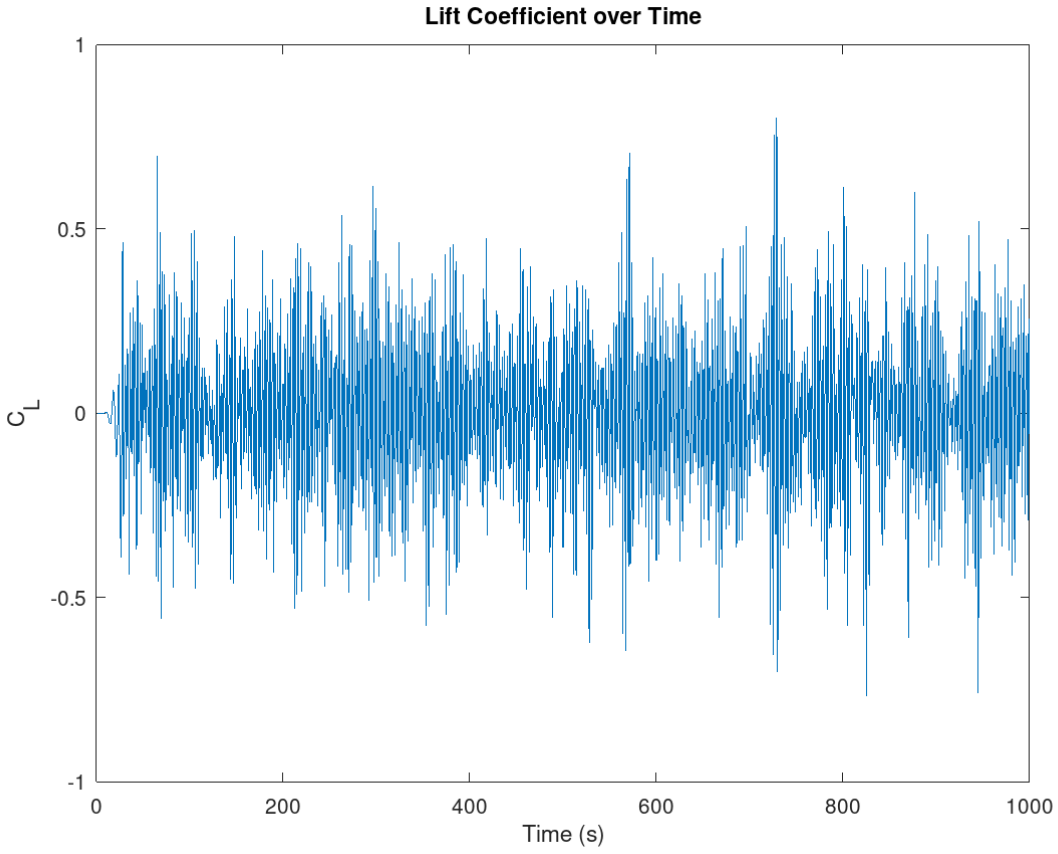


Figure 5.12: Plot of lift coefficient over total simulated time (1000 s)

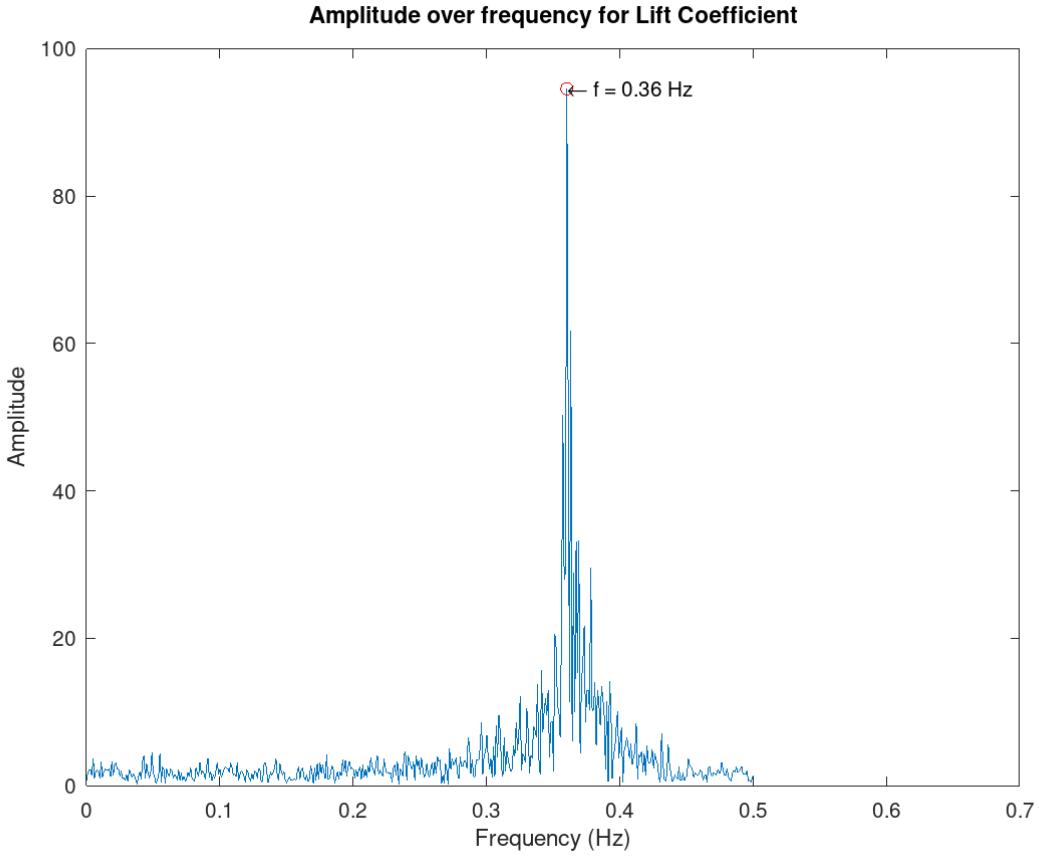


Figure 5.13: FFT of the lift coefficient

After performing the FFT, we see that the maximum amplitude is located at $f_s = 0.36\,\text{Hz}$, therefore this is the vortex shedding frequency, and the resulting Strouhal number is $Sr = 0.23$.

# Conclusion

In Deliverable Task I, the flow over a circular cylinder was studied by CFD, using the pimpleFoam solver of OpenFOAM. The effect of mesh resolution on the simulation results and the influence of relaxation factors on the simulation runtime were also studied as preliminaries. The Smagorinsky subgrid-scale model captures the unsteady phenomenon of vortex shedding and the formation of the Karman vortex street, and several results were extracted by post-processing after a total simulated time of 1000 s.

# Bibliography


[1] OpenCFD Ltd. OpenFOAM Extended Code Guide v2012, 2020.

[2] NPARC Alliance CFD Verification and Validation Web Site. Examining Spatial (Grid) Convergence.

[3] E.S.D.U. Fluid forces on non-streamline bodies - background notes and description of the flow phenomena. ESDU, 71012.

[4] Boyun Guo, Shanhong Song, Ali Ghalambor, and Tian Ran Lin. Chapter 18 - pipeline vibration and condition based maintenance. In Boyun Guo, Shanhong Song, Ali Ghalambor, and Tian Ran Lin, editors, Offshore Pipelines (Second Edition), pages 299–337. Gulf Professional Publishing, Boston, second edition edition, 2014.

[5] Miguel Mendez, Massimiliano Nardo, and Carlo Benocci. Running fineopen43 simulations at vki: A tutorial and a collection of scripts. 03 2017.